CHAPTER 6

RESULTS AND DISCUSSION: PHOSPHATE REMOVAL BY SLAG

6.1. Particle dimensions and chemical composition

The particle size distribution for the slag, obtained by Fraunhofer diffraction particle analysis as described in Experimental Section 4.3.1, is illustrated in Figure 6.1.

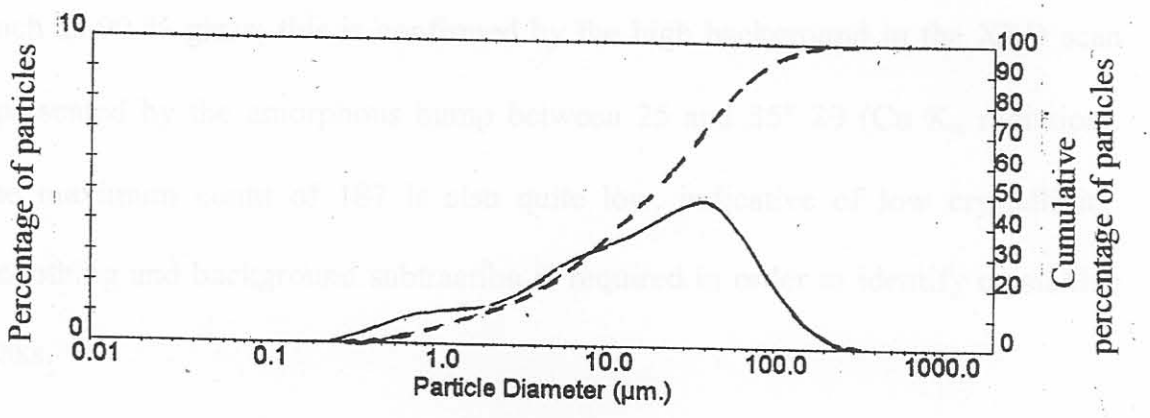

Figure 6.1. Particle size distribution for the slag sample.

The solid line represents the percentage of particles having a given diameter, the particle size distribution being a logarithmic function of the individual particle sizes (see equation (3.1)). The broken line is a cumulative curve that represents the percentage of particles whose diameters are less than a given diameter. About 57% of the particles were found to have diameters in the 5-50 µm size range.

Table 6.1 represents a summary of some important physical characteristics.

Table 6.1. Physical properties of slag.

Characteristic	Value
Specific surface area (m^2/g)	1.29
Mean particle diameter $d_{4,3}$ (μm)	31.4
Density (g/cm^3)	2.82

The raw XRD pattern is shown in Figure 6.2(a). Slags are known to contain as much as 90 % glass; this is confirmed by the high background in the XRD scan represented by the amorphous hump between 25 and 35° 2θ (Cu K_α radiation). The maximum count of 187 is also quite low, indicative of low crystallinity. Smoothing and background subtraction is required in order to identify crystalline peaks.

Figure 6.2(b) shows the smoothed and background-subtracted pattern. The main crystalline phase appears to be tricalcium silicate (C_3S) with relatively prominent peaks at 29.5, 34.5, 41.5, and 52° 2θ, synonymous with the main phase in OPC.

The chemical oxide composition obtained by XRF is shown in Table 6.2. Lime, silica, alumina and magnesia are evident as the four major constituents of the slag sample used.

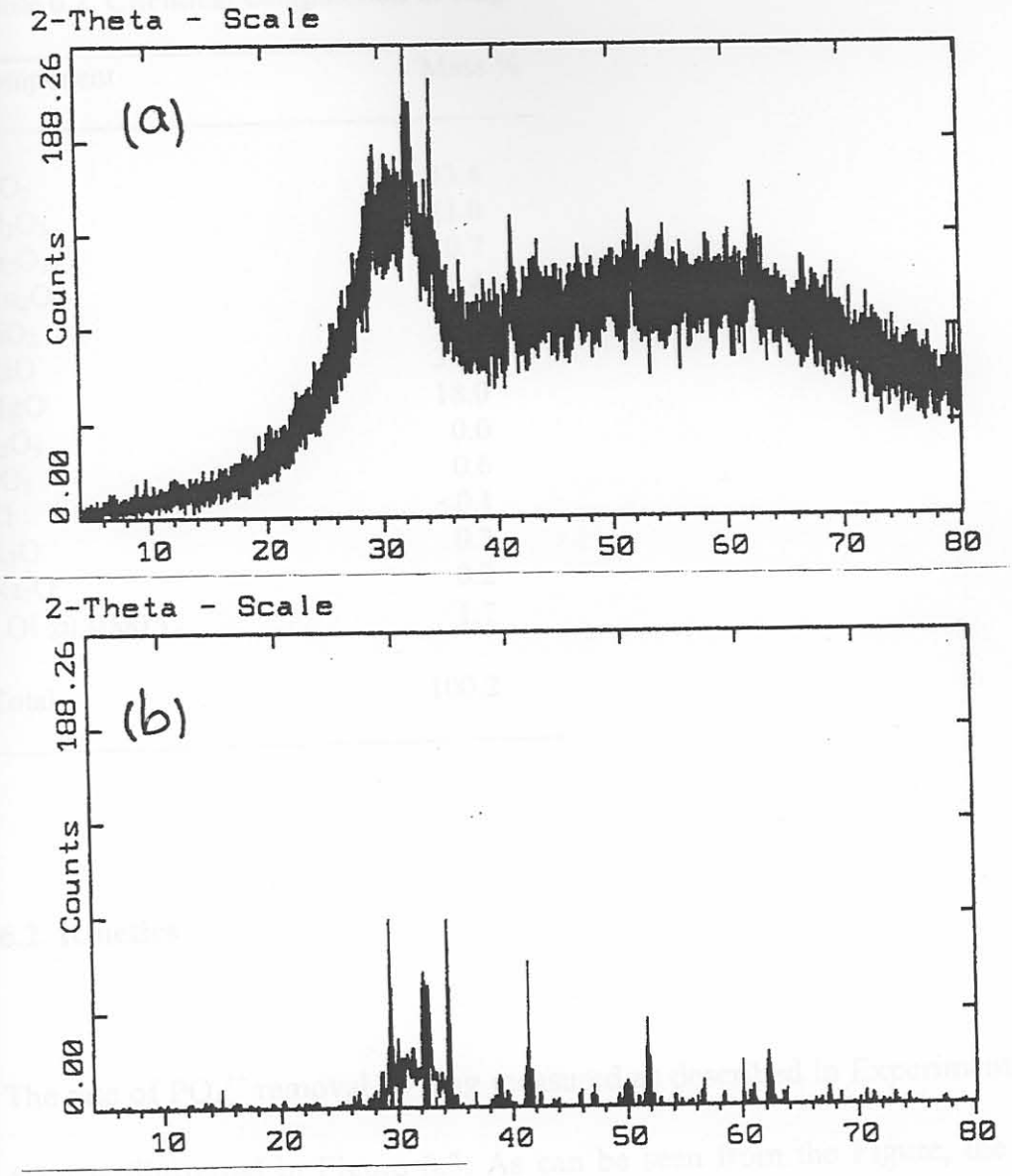

Figure 6.2. Diffractogram of the slag sample: (a) raw pattern (b) smoothed and background subtracted pattern.

Table 6.2. Chemical composition of slag.

Component	Mass %
SiO_2	33.4
Al_2O_3	11.0
Fe_2O_3	0.7
Mn_2O_3	0.4
TiO_2	0.6
CaO	33.3
MgO	18.0
P_2O_5	0.0
SO_3	0.6
Cl	<0.1
K_2O	0.3
Na_2O	0.2
LOI @ 1000°C	1.7
Total	100.2

6.2. Kinetics

The rate of PO_4^{3-} removal by slag measured as described in Experimental Section 4.3.4 is illustrated in Figure 6.3. As can be seen from the Figure, the uptake of PO_4^{3-} approaches a limiting value of ca 65 % after a contact time of ca 4 hrs, signalling the attainment of dynamic equilibrium conditions. The fractional attainment of equilibrium as a function of time, assuming a first order reversible kinetics model, is given by equation (1.12) as explained in Section 1.3.

A plot according to equation (1.12) is shown in Figure 6.4.

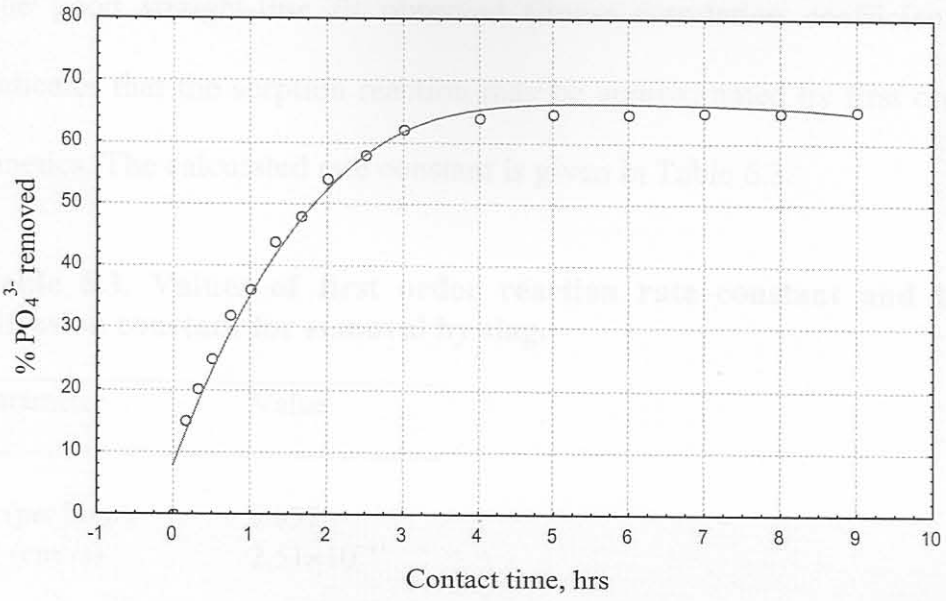

Figure 6.3. Kinetics of PO_4^{3-} removal by slag. (Conditions: 2 g slag, 80 mg/l PO_4^{3-}-P, pH 9.0, 25°C)

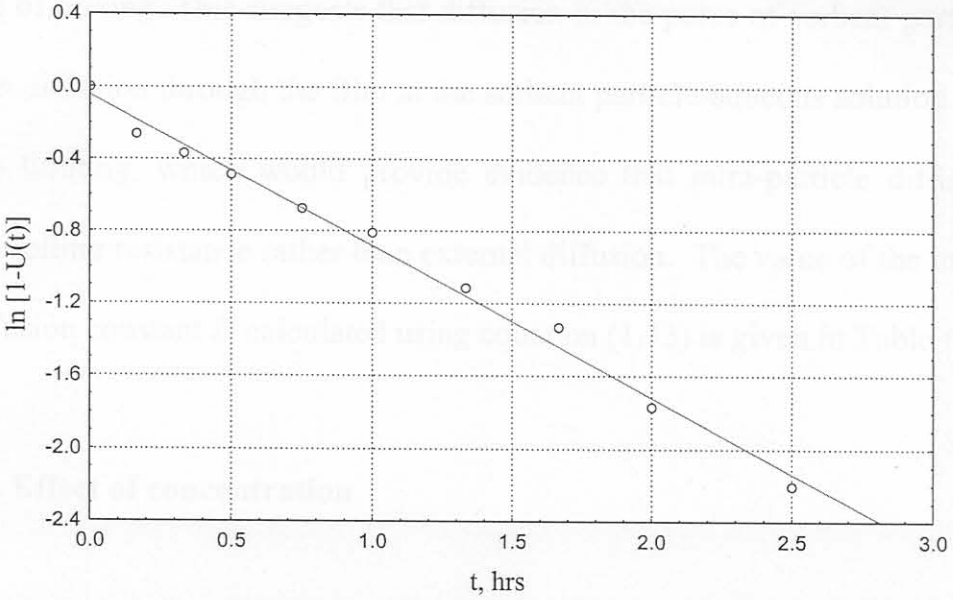

Figure 6.4. Application of first order kinetics to the experimental adsorption data for slag. (Conditions: 2 g slag, 80 mg/l PO_4^{3-}-P, pH 9.0, 25°C)

The good straight-line fit observed (linear correlation coefficient R^2= 0.992) indicates that the sorption reaction may be approximated by first order reversible kinetics. The calculated rate constant is given in Table 6.3.

Table 6.3. Values of first order reaction rate constant and intra-particle diffusion constant for removal by slag.

Parameter	Value
k' (per hour)	0.837
D (cm^2/s)	2.51×10^{-11}

Over the range of sorbent-solution agitation rates studied (100-140 cycles per minute horizontally) it was observed that the sorption rate was not affected by the rate of mixing. This suggests that diffusion in the pores of sorbent particles rather than diffusion through the film at the sorbent particle-aqueous solution interface is rate limiting, which would provide evidence that intra-particle diffusion is the controlling resistance rather than external diffusion. The value of the intra-particle diffusion constant D calculated using equation (1.13) is given in Table 6.3.

6.3. Effect of concentration

Figure 6.5 illustrates the effect of concentration on the efficiency of PO_4^{3-} removal, measured as described in Experimental Section 4.3.5.1.

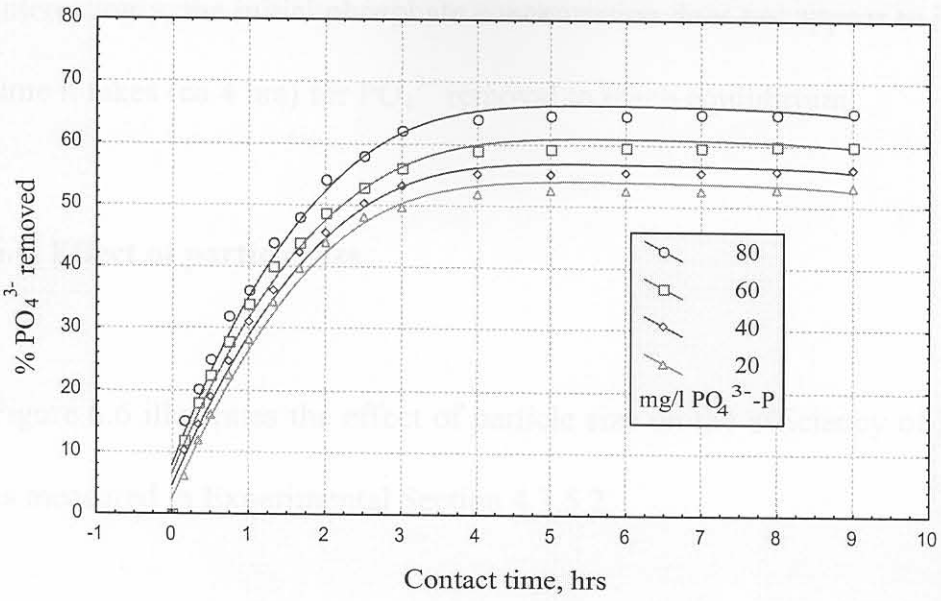

Figure 6.5. Effect of concentration on the kinetics of PO_4^{3-} removal by slag. (Conditions: 2 g slag, pH 9.0, 25°C)

The rate of removal and separation efficiency of PO_4^{3-} from aqueous solution by slag was found to increase with the initial phosphate concentration over the concentration range studied.

The observed increase in the percentage PO_4^{3-} removed with increasing solute concentration (for the same amount of slag) is hardly surprising if the system under study is non-ideal. As mentioned in Sections 1.2.1 and 1.2.2, for non-ideal systems the mass of solute adsorbed per mass of sorbent keeps increasing as the concentration of the solute increases. This has been ascribed to surface heterogeneity in such systems.

Interestingly, the initial phosphate concentration does not appear to influence the time it takes (ca 4 hrs) for PO_4^{3-} removal to reach equilibrium.

6.4. Effect of particle size

Figure 6.6 illustrates the effect of particle size on the efficiency of PO_4^{3-} removal as measured in Experimental Section 4.3.5.2.

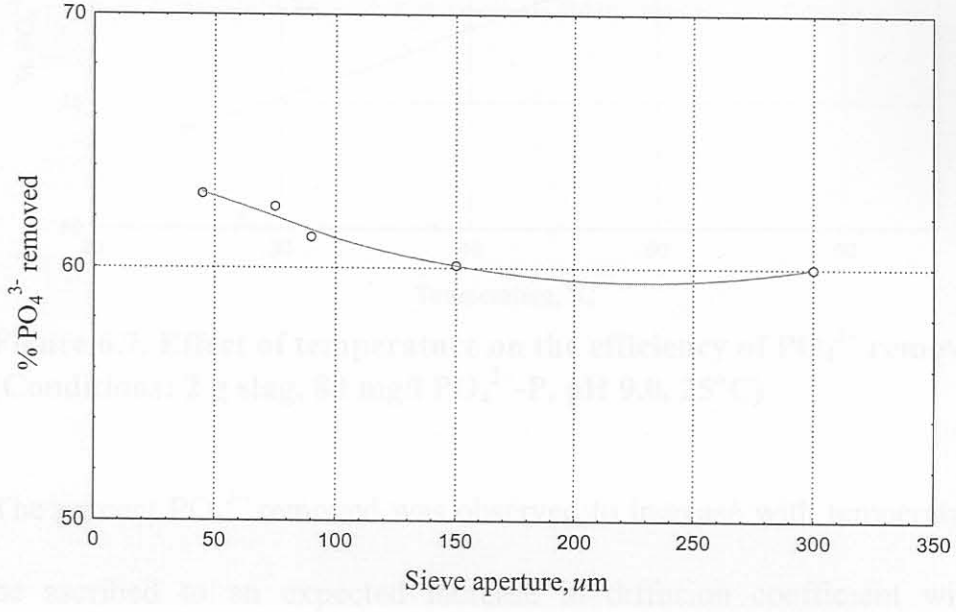

Figure 6.6. Effect of particle size on the efficiency of PO_4^{3-} removal by slag. (Conditions: 2 g slag, 80 mg/l PO_4^{3-}-P, pH 9.0, 25°C)

Although there was some increase in the percentage PO_4^{3-} removed as the particle size decreased, this increase does not appear to be proportional to the increased surface area.

6.5. Effect of temperature

The effect of temperature on the efficiency of PO_4^{3-} removal measured as described in Experimental Section 4.3.5.3 is illustrated in Figure 6.7.

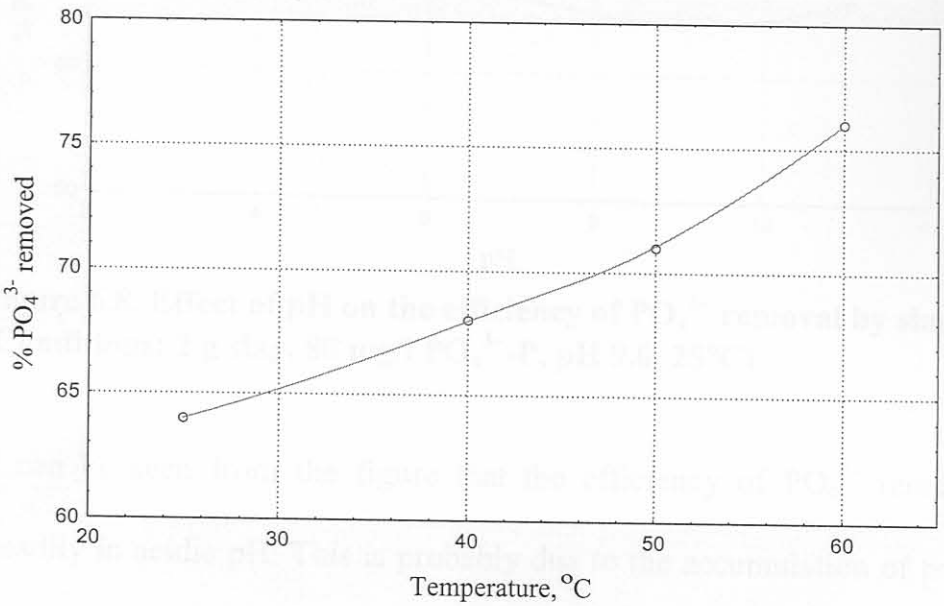

Figure 6.7. Effect of temperature on the efficiency of PO_4^{3-} removal by slag. (Conditions: 2 g slag, 80 mg/l PO_4^{3-}-P, pH 9.0, 25°C)

The percent PO_4^{3-} removed was observed to increase with temperature. This may be ascribed to an expected increase in diffusion coefficient with increasing temperature.

6.6. Effect of pH

Figure 6.8 illustrates the variation of percent PO_4^{3-} removed with the initial pH of the aqueous solution, measured as described in experimental Section 4.3.5.4.

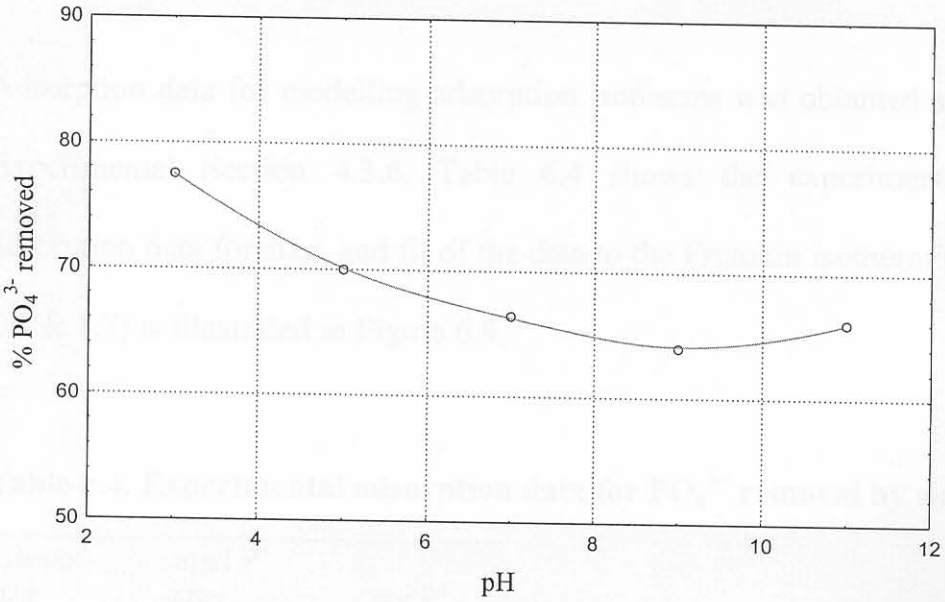

Figure 6.8. Effect of pH on the efficiency of PO_4^{3-} removal by slag. (Conditions: 2 g slag, 80 mg/l PO_4^{3-}-P, pH 9.0, 25°C)

It can be seen from the figure that the efficiency of PO_4^{3-} removal increases steadily in acidic pH. This is probably due to the accumulation of positive charge on the adsorbent surface that increases its affinity for the negatively charged phosphate ions. The observed slight increase in the efficiency of PO_4^{3-} removal beyond pH 9 could be due to the creation of favourable conditions for calcium phosphate precipitation at high pH, thus enhancing the removal of PO_4^{3-} by some dissolved calcium formed by hydration of slag, or being present in the slag as free lime.

6.7. Adsorption isotherms

Adsorption data for modelling adsorption isotherms was obtained as described in Experimental Section 4.3.6. Table 6.4 shows the experimentally obtained adsorption data for slag, and fit of the data to the Frumkin isotherm (see equations 1.6 & 1.7) is illustrated in Figure 6.9.

Table 6.4. Experimental adsorption data for PO_4^{3-} removal by slag.

mass of slag (g)	mg/l P[a] after adsorption	mg P[a] adsorbed
0.5	48.5	10.3
2	46.7	10.6
3	45.8	10.8
3.5	43.5	11.3
4	33.7	13.3
5	21.7	15.7

[a] PO_4^{3-} (as P)

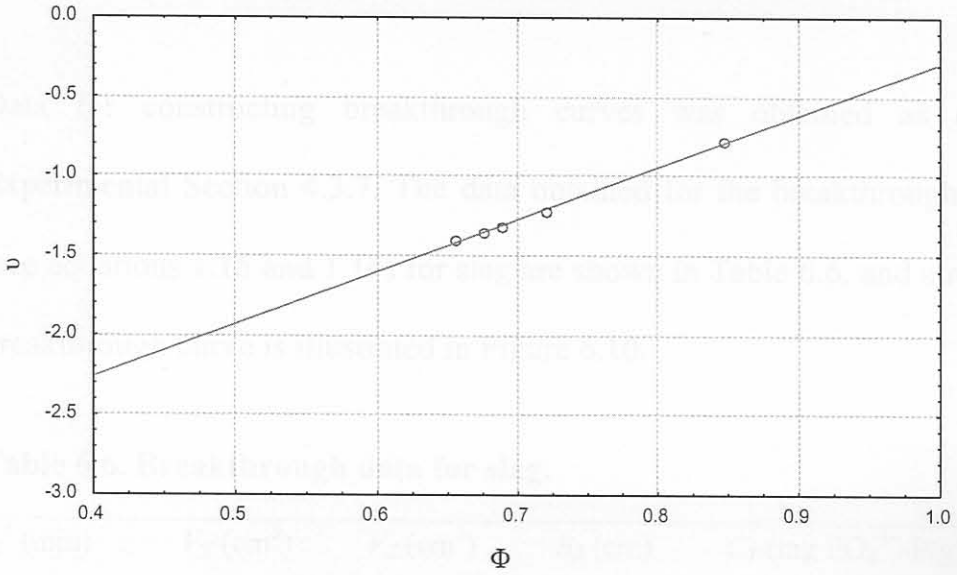

Figure 6.9. Application of the Frumkin equation to the experimental adsorption data (given in Table 6.4) for slag.

Attempts to fit the data to the Langmuir (equation 1.3) and Freundlich (equation 1.4) isotherms yielded non-linear plots with values of $R^2 < 0.3$. It is evident that the Frumkin isotherm (equation 1.7) is the appropriate one for fitting the data, which is indicative of a non-ideal system with finite lateral interactions among adsorbate particles. The Frumkin constants were calculated and are shown in Table 6.5.

Table 6.5. Isotherm linear correlation coefficients and Frumkin constants for PO_4^{3-} adsorption by slag.

Isotherm	R^2	α	β
Frumkin	0.997	3.780	0.015
Langmuir	0.270		
Freundlich	0.233		

6.8. Breakthrough curves

Data for constructing breakthrough curves was obtained as described in Experimental Section 4.3.7. The data obtained for the breakthrough experiments (see equations 1.15 and 1.16) for slag are shown in Table 6.6, and a representative breakthrough curve is illustrated in Figure 6.10.

Table 6.6. Breakthrough data for slag.

t_E[a] (min)	V_T (cm^3)	V_Z (cm^3)	h_Z (cm)	C_T (mg PO_4^{3-}-P/g)
7.0	312	138	1.133	60

[a]Breakthrough time

The curves obtained were good approximations for characteristic symmetrical breakthrough S curves. Average values obtained for the breakthrough time t_E, the effluent volume required for bed exhaustion V_T, V_Z (V_T minus the effluent volume required for breakthrough), the height of the mass transfer zone h_Z, and the adsorption capacity C_T are given in Table 6.6.

An average capacity value C_T of 60 mg PO_4^{3-}-P/g slag was obtained.

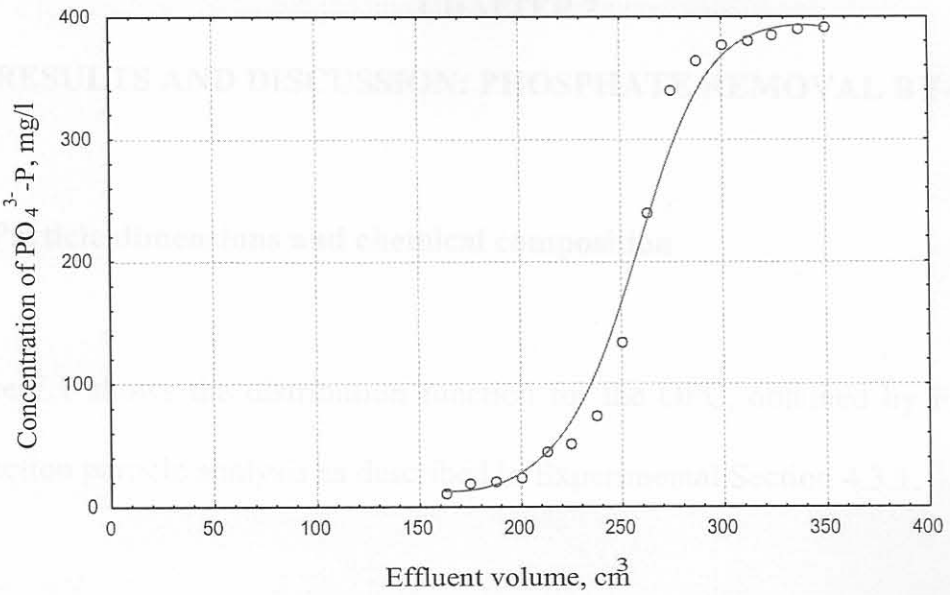

Figure 6.10. Breakthrough curve for removal by slag.